Received: 12 February 2019 | Revised: 2 April 2019 | Accepted: 1 May 2019

DOI: 10.1111/jace.16536

ORIGINAL ARTICLE

Journal of the American Ceramic Society

Computational insights into the structure of barium titanosilicate glasses

El Mehdi Ghardi[1] | **Achraf Atila**[2] | **Michael Badawi**[3] | **Abdellatif Hasnaoui**[4] | **Said Ouaskit**[1]

[1]Laboratoire physique de la matière condensée (LPMC), Faculté des sciences Ben M'sik, Université Hassan II Casablanca - UH2C, Casablanca, Morocco

[2]Department of Materials Science and Engineering, Institute I, Friedrich-Alexander-Universität Erlangen-Nürnberg (FAU), Erlangen, Germany

[3]Laboratoire de Physique et Chimie Théoriques, UMR 7019, Université de Lorraine - CNRS, Nancy, France

[4]LS3M, Faculté Polydisciplinaire de Khouribga, Université Sultan Moulay Slimane, Khouribga, Morocco

Correspondence
El Mehdi Ghardi, Laboratoire physique de la matière condensée (LPMC), Faculté des sciences Ben M'sik, Université Hassan II Casablanca - UH2C (Morocco).
Email: mehdighardi94@gmail.com
and
Abdellatif Hasnaoui, LS3M, Faculté Polydisciplinaire de Khouribga, Université Sultan Moulay Slimane - B. P.: 145, 25000 Khouribga, Morocco.
Email: hasnaoui59@hotmail.com

Abstract

Understanding the role of TiO_2 in BaO-TiO_2-SiO_2 (BTS) glasses is one of the keys to develop new glasses and glass-ceramics for different technological applications. For the first time, molecular dynamics simulations were conducted to get new insights into the atomic structure of the BTS glasses and their elastic moduli. Various compositions are studied where SiO_2 have been replaced by TiO_2. The calculated mechanical properties of our models are observed to depend linearly on TiO_2 content. However, the structure-induced changes are far from such dependence. The structural results indicate that BTS glasses are mainly built on four types of basic units: SiO_4, TiO_4, TiO_5 and TiO_6. This high structural heterogeneity induced by the three coordination states of Ti is found to have an impact on the medium range order by increasing the rings number, the polymerized regions, and by transforming Q_3-Q_4 and Q_2 without neglecting the increase in Q_5 and Q_6 species. Those structural modifications of the BTS glass network features have been found to be consistent with available experimental data.

KEYWORDS

BaO-TiO_2-SiO_2, elastic properties, molecular dynamics, structural properties, titanosilicate glass

1 | INTRODUCTION

Glass-ceramics are engineering materials with special properties arising today in the development of new and innovative technologies. They are defined as composite materials constituted of crystals in a glassy matrix,[1] showing favorable thermal, chemical, biological, and dielectric properties, generally superior to metals and organic polymers in these areas. These materials have opened a wide range of practical applications.[2]

An emerging glass-ceramics system that has gathered a tremendous scientific and industrial interest is the Barium Titanosilicate BaO-TiO_2-SiO_2 (BTS). Mainly due to its $Ba_2TiSi_2O_8$ fresnoite crystalline phase,[3] BTS glass-ceramics have shown promising properties especially noting pyroelectricity, piezoelectricity, photoluminescence,[4] and nonlinear optical properties that result from the crystal polarity. Also, many potential applications have been reported for the BTS system such as the immobilization of short-lived fission products in radioactive waste.[5] Moreover, they can be used in catalysts, ion-exchangers or optical devices.[5–8] The relative availability of the BTS constituting elements was considered to justify these scientific efforts from both environmental and economic point of view.[9] One possible way to explain the remarkable properties of the BTS has been found by Roberts et al.[7] In over 100 titanosilicate minerals they have reported that in only

one of them Titanium (Ti) takes up fivefold coordination, and that was in BTS-fresnoite. The origin of the intriguing properties of the BTS has been then related to the square pyramidal TiO_5 polyhedra present in the BTS-fresnoite that makes it highly polar.[10]

The BTS system has also some contribution to the fundamental aspects of the glass science. During the surface crystallization of glasses, oriented nucleation was first detected after the surface crystallization of Ba-fresnoite from a glass.[11] This observation is in contrast to the basic assumption of randomly oriented nuclei in the classical nucleation theory for glasses.[3] A second contribution can be also considered which is related to the distribution of excess in the vibrational density of states. Nakamura et al[12] have reported previously that the excess in the vibrational density of states in the glassy fresnoite is considerably similar to that of the crystalline counterpart with the same stoichiometry which can be useful to understand the origin of boson peak.

The BTS glass-ceramics can be made from glass precursors with different nominal compositions submitted to a heat treatment. The crystallization behavior of glass-ceramics depends strongly on the composition of the glass as well as the heat-treatment conditions.[13] Many authors have studied the glass crystallization tendency and its consequences on the glass ceramic properties,[13–15] however only few were interested on the glassy BTS.[16–18] Owing to the fact that Ti is a main component of BTS, playing an important role in giving its most promising properties as mentioned before, we will focus in this work on TiO_2 effect in the glassy BTS.

One way to study glasses is to understand the structure-property relationship as a function of chemical composition and temperature. In fact, finding such a relationship has been recognized as the main goal of the glass science.[19] To achieve that goal, atomistic simulations have taken a large part in these types of studies due to their ability to access high and low temperature phenomena. During the last decades, classical molecular dynamics simulations have proven their efficiency in reproducing, modeling materials, and probing the origin of their properties at the atomic scale in many fields. Indeed these techniques have been successfully applied in studying the local atomic structural order in silica-based glasses[20,21] and in metallic glasses.[22–24] Here, based on molecular dynamics simulation, we present a study of the barium titanosilicate glass BTS to characterize some correlation between the role of TiO_2 in improving the glass elasticity and the structural properties for a large composition range. To the best of our knowledge, this is the first atomistic study reported on the BTS glasses.

2 | COMPUTATIONAL PROCEDURE

2.1 | Glass preparation

Molecular dynamics simulation was performed on $(BaO)_{0.3}(TiO_2)_x(SiO_2)_{(0.7-x)}$ glass system for seven compositions ($x = 0, 0.05, 0.10, 0.15, 0.20, 0.25, 0.30$) where SiO_2 content was replaced by TiO_2. For each composition, a total number of 2500 atoms were placed randomly in a cubic simulation box ensuring that there is no overlapping between atoms. The atomic compositions and the simulation cubic box cell parameters are reported in Table 1. All MD simulations were performed using the LAMMPS[16] package. The integration of equations of motion was performed using the Verlet-velocity algorithm with a time step of 2 fs, this time step is chosen to shorten the simulation time without altering the properties of the glass. Periodic boundary conditions were applied in all directions to avoid edge effects and to simulate a bulk system.

To model the interatomic interaction in the BTS system, a rigid ionic model with partially ionic charge proposed by Pedone et al[25] was used. The potential energy is constructed by three different contributions: (a) a long-range Coulombic interaction; (b) a short-range interaction described by the Morse function; and (c) a short-range repulsive term which was added to model the repulsive contribution at high temperature and pressure. The potential used in our modeling is expressed as follows:

$$U_{ij}(r) = \frac{z_i z_j e^2}{r} + D_{ij}\left[\left(1-\exp\left(-a_{ij}\left(r-r_{ij}\right)\right)\right)^2 - 1\right] + \frac{C_{ij}}{r^{12}} \quad (1)$$

TABLE 1 Number of atoms, densities, and cubic box cell parameters for different simulated glasses. N_o, N_{Si}, N_{Ba}, and N_{Ti} stand for the number of O, Si, Ba, and Ti atoms, respectively

TiO_2 (%)	N_O	N_{Si}	N_{Ba}	N_{Ti}	Total atoms	Cubic Box cell parameter (Å)	ρ (g/cm^3)
0	1574	648	278	0	2500	33.50	3.60
5	1574	602	278	46	2500	33.44	3.66
10	1574	555	278	93	2500	33.30	3.75
15	1574	509	278	139	2500	33.27	3.83
20	1574	463	278	185	2500	33.09	3.90
25	1574	417	278	231	2500	33.14	3.93
30	1574	370	278	278	2500	33.01	4.02

with z_i and z_j are the partial ionic charges of atoms i and j respectively D_{ij}, a_{ij}, r_{ij} and C_{ij} are the potential parameters (see Table 2). The Coulombic interactions were evaluated using the Ewald summation method with a cutoff of 12 Å and a precision of 10^{-6}. The short-range interaction cutoff distance was chosen to be 5.5 Å. Indeed, the values of the cutoff have an important role on the quality of the obtained results and the energy convergence, thus we did choose values that are often used in the literature.[25]

The samples were heated and equilibrated at a temperature equal to 4000 K for 1 ns in the NVT ensemble, this step is needed to obtain an equilibrated melt and to ensure that the system loses its initial configuration memory. After that, the systems were subjected to a linear cooling in the NVT ensemble from 4000 K to 300 K using a cooling rate of 1 K/ps. Finally, we did also run another 100 ps for statistical averaging in the NVT ensemble. It is also known that the cooling rate used in molecular dynamics is several orders of magnitude higher than those used in experiments, which is due to the limitation of molecular dynamics to use the experimental cooling rates and the computational power to do that is very expensive. Therefore, our value of cooling rate is in the range of those used in works studying glasses through the melt quenching technique in MD.[26,27]

2.2 | Computation of structural and elastic properties

2.2.1 | Radial distribution function

The radial distribution function (RDF) $g(r)$ is widely used to describe the structural characteristics of any spatial distribution of atoms found in materials.[28] Considering a particle to be at the origin, knowing the number of particles $dn(r)$ at a distance between r and $r + dr$, $g(r)$ represents the probability of finding another particle within an infinitesimal region of space dr at a distance r from the particle at the origin. The $g(r)$ can be expressed as follows:

$$g(r) = \frac{dn(r)}{4\pi r^2 \rho dr} \tag{2}$$

For multicomponent systems, the partial radial distribution (PDF) $g_{\alpha\beta}(r)$ function calculates the probability of finding a particle β at a distance from a particle α at the origin.

TABLE 2 Potential parameters used in this study

	D_{ij} (eV)	a_{ij} (Å^{-2})	r_{ij} (Å)	C_{ij} (Å^{12})
$O^{-1.2}$-$O^{-1.2}$	0.042395	1.379316	3.618701	22.0
$Ba^{+1.2}$-$O^{-1.2}$	0.065011	1.547596	3.393410	5.0
$Si^{+2.4}$-$O^{-1.2}$	0.340554	2.006700	2.100000	1.0
$Ti^{+2.4}$-$O^{-1.2}$	0.024235	2.254703	2.708943	1.0

2.2.2 | Static structure factor

The structure factor is a mathematical tool that describes the way a material can scatter radiation. In numerical studies, it can be computed by using the Debye equation or by simply Fourier transform the radial distribution function. This latter method is widely used to allow a direct comparison between experiments and simulation. In this work, the static structure factor is mainly used to study the medium range order. The expression of the structure factor is given by the following equation:

$$S(q) = 1 - \rho \int_0^\infty (g(r) - 1) \exp(iqr) dr \tag{3}$$

Where q is the wave vector and ρ is the particle density. The partial structure factor was also computed using Faber-Ziman formalism[29] that allows the decomposition of the total structure factor into partial contributions between different pairs of species. The partial structure factor using Faber-Ziman formalism is expressed as follows:

$$S^{FZ}_{\alpha\beta}(q) = 1 + 4\pi\rho \int_0^\infty \left(g_{\alpha\beta}(r) - 1\right) r^2 \frac{\sin(qr)}{qr} dr \tag{4}$$

where $g_{\alpha\beta}(r)$ represents the partial radial distribution function. The total structure factor can be obtained by the relation:

$$S(q) = \sum\nolimits_{\alpha\beta} c_\alpha b_\alpha c_\beta b_\beta \left[S^{FZ}_{\alpha\beta} - 1\right] \tag{5}$$

2.2.3 | Ring statistics

Rings are often used to characterize the medium range structure in glasses; there are many definitions depending on the criterion used to calculate them.[30–32] To compute the ring size distribution, we have used the simplest definition which considers rings as the shortest closed paths within the glass network which are called primitive rings.[31] The computation of ring size distribution in the barium titanosilicate glass was performed using the Rings code.[33]

2.2.4 | Elastic properties

Every material can be deformed without breaking when external forces are applied while not exceeding the limit of small deformations. This ability is defined as the material elasticity.[34] One way to characterize a material elasticity is to calculate the stiffness matrix. Once obtained, several mechanical properties as bulk modulus (B), shear modulus (G), and Young modulus (E) can be easily derived. The potential energy second derivative is a commonly used method to compute the stiffness matrix. This method computes the elastic constants from the curvature of the energy surface minimum

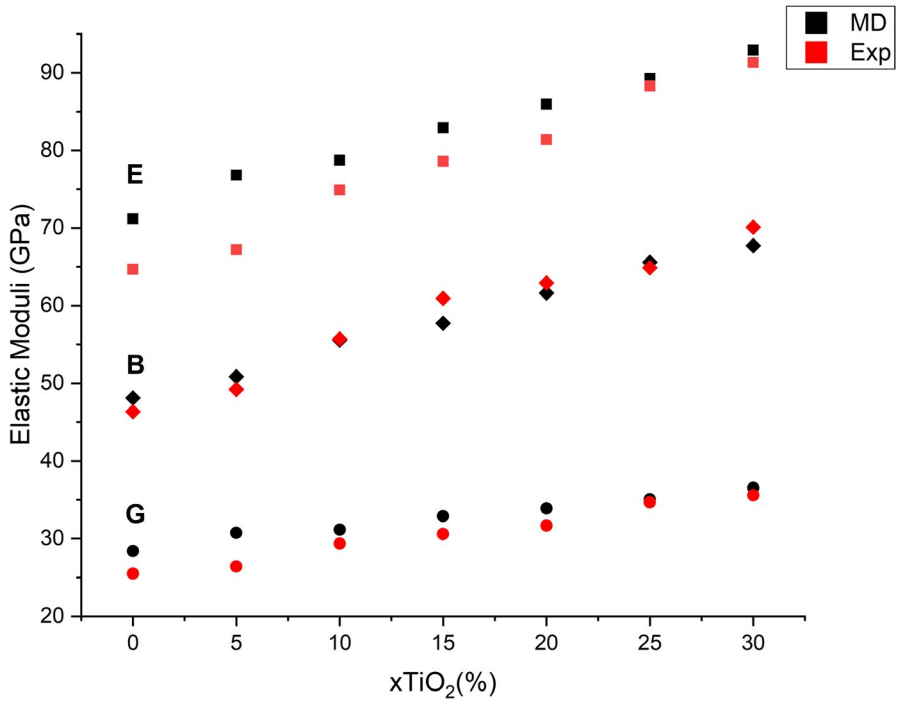

FIGURE 1 Bulk (B), shear (G), and Young's (E) moduli for the different glass compositions compared with experimental data[17] [Color figure can be viewed at wileyonlinelibrary.com]

by deriving at the second-order potential energy density with respect to the strain. The elements of the stiffness matrix are expressed by the following expression:

$$C_{ij} = \frac{1}{V}\left(\frac{\partial^2 U}{\partial \in_i \partial \in_j}\right) \tag{6}$$

This method uses molecular statics simulations at 0 K. Structures at mechanical equilibrium are subject to six tensile and six shear deformations. After each deformation, the new generated configurations are minimized to reach their local minima and the changes measured in the stress tensor are computed.

In isotropic materials, the elastic properties are computed using the following relations:

$$\bullet \text{Bulk modulus}: \quad B = \frac{C_{11} + 2C_{12}}{3} \tag{7}$$

$$\bullet \text{Shear modulus}: \quad G = C_{44} \tag{8}$$

$$\bullet \text{Young modulus}: \quad E = \frac{9BG}{3B + G} \tag{9}$$

3 | RESULTS AND DISCUSSION

3.1 | Glass elasticity

The effect of TiO_2 content on elastic properties of BTS glasses is shown in Figure 1. Based on our simulations, adding TiO_2 into the glass network affects its elasticity by increasing the Young modulus (E), the bulk modulus (B), and the shear modulus (G). The used interatomic potential to model the network of the BTS glass is satisfying since the behavior of the elastic moduli as a function of the TiO_2 content is in a realistic agreement with the available experimental data. However, a slightly overestimation of Young modulus is observed for low TiO_2 contents but this can be considered in the range of the relative error whose maximum is estimated to be 13%. This can be a direct consequence of performing simulations with adjusted densities to the experimental ones during the cooling schedule, that type of simulation produces glasses under high pressure which can induce this overestimation in our results.[35] Nevertheless, the overall experimental behavior of elastic properties is well reproduced in our simulations. The trend observed for Young modulus can be mainly due to the increase in the connectivity of the glass network. In fact, the young modulus is determined by the individual bonds in the material and by the structure of the network.[36] The Bulk modulus shows also the same trend by continuously increasing the TiO_2 content. This might be due to the decrease in the total free volume observed with the increase in density of packing atoms in the structure. Consequently, this will lead to the lowering of glass compressibility and promoting glass cohesion. In addition to that, and as illustrated in Figure 1, the shear modulus behaves in a similar way as the Young's and the bulk moduli with increasing TiO_2 content in the glass. The shear modulus defines the elastic behavior of a material under a shear stress. Because of the close relation between the Young modulus and the shear modulus, the same trend can be observed comparing to experimental data.

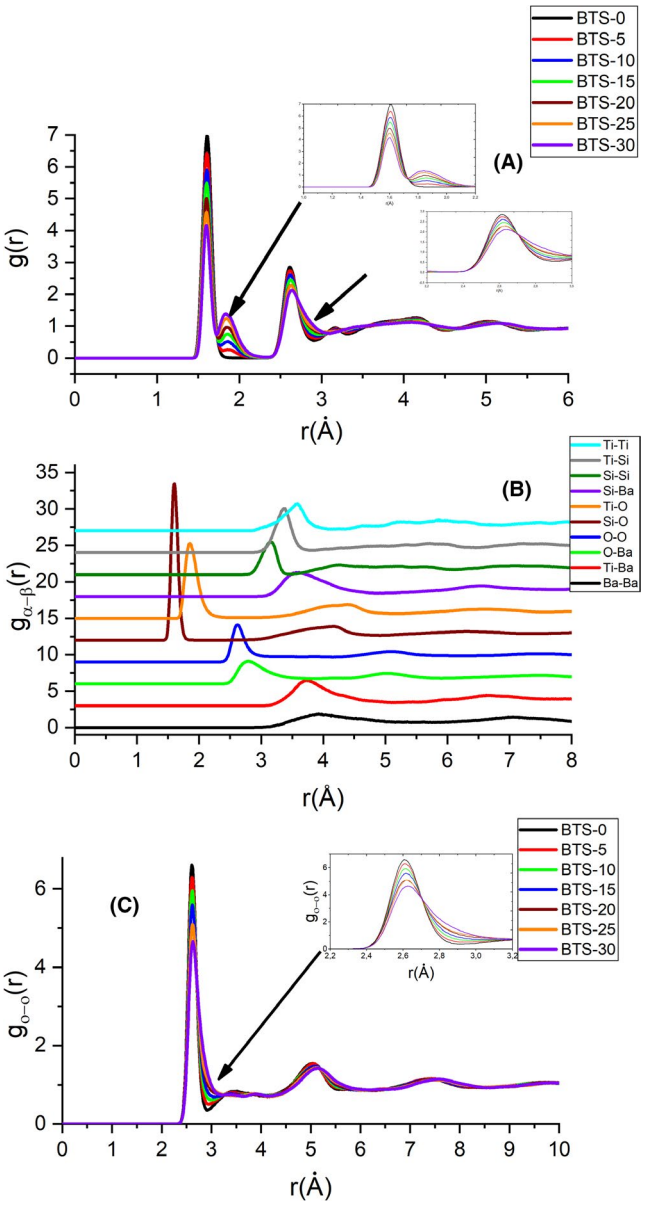

FIGURE 2 (A), Simulated total radial distribution functions for the different used BaO-TiO_2-SiO_2 (BTS) glass compositions, (B) partial distribution functions for the glass composition $x = 20\%$ and (C) O-O radial distribution functions for the different used BTS glass compositions. The insets are enlarged portions of different indicated zones in (A,C) [Color figure can be viewed at wileyonlinelibrary.com]

The effect of TiO_2 content on mechanical properties in silicate glasses is captivating because of its complicated nature. The glass with the highest content of TiO_2 showed higher elastic moduli. The stiffness of this glass has increased with 30% proportionally to the TiO_2 content but adding TiO_2 is not the direct reason for this increase in mechanical properties. In the binary SiO_2-TiO_2 glass, an opposite effect was demonstrated by Scannell et al.[37] A decrease in the elastic moduli was observed when increasing TiO_2 content up to 10%. In the absence of network modifier and with the same range of TiO_2 composition, Sandstrom et al[38] reported previously that the structure of the SiO_2-TiO_2 glass was mainly build on fourfold coordinated Ti. In a ternary glass with the presence of a modifier, Scannell et al[39] have studied structural and mechanical properties of Na_2O-TiO_2-SiO_2 ternary glass and have found that the fivefold coordinated Ti cations begin to appear at low-TiO_2 content and dominate for higher percentages. The increase in the mechanical properties was directly observed independently of the sodium-modifier content. The ability of TiO_2 to increase glass mechanical properties depends strongly on Ti coordination that defines the role of TiO_2 in the glass network. The presence of modifier is also required to occupy the network-free volume and to charge balance the Ti environment in high coordination states.

Summarizing our findings, the very nice agreement between our computed mechanical properties with the experimental ones (See Figure 1) strongly validates our force-field approach. This allows us to further investigate in details the structural properties of the BTS glasses.

3.2 | Structural properties

3.2.1 | Short-range order

A well-known fact about the structure of silicate glasses networks is that they are built on corner sharing tetrahedral structural unit of SiO_4.[19] The variation in the Si-O bond length and the O-Si-O angle which characterizes the shape of these structural units has an important impact on the glass properties. To study the effect of TiO_2 on the short-range structure of the BTS glass (distances <4 Å), we first calculated the total RDF $g(r)$. Figure 2 shows the RDFs for different glass composition (a), the PDFs of the glass with 20% of TiO_2 (b) and the PDFs of O-O pair for all compositions (c).

In Figure 2A, the effect of TiO_2 on the structure of the BTS glass is mainly observed in the first three peaks for a distance lower than 3 Å. The first peak is identified as the contribution of the Si-O bond in the BTS glass, its intensity decreases with increasing TiO_2 content. The second peak, which represents the Ti-O bond contribution in the network (Figure 2A) has the shape of a growing shoulder with increasing TiO_2 and can be considered as a consequence for the decrease in intensity of the first peak since TiO_2 is replacing SiO_2. The third peak represents a superposition of both Ba-O and O-O bonds contributions in the BTS glass network as confirmed by the PDF in Figure 2B, where the positions of the main peaks of $g_{Bao}(r)$ and $g_{oo}(r)$ corresponds to the Ba-O and O-O bond lengths. In the zoom-in of the third peak in Figure 2A, two main features were mainly observed and attributed to the effect of TiO_2: the first one is related to the decrease in the peak intensity and the second one is presented by the shift in the first peak minimum toward higher values with increasing TiO_2. The behavior of O-O PDFs as a function of composition observed in Figure 2C is similar to the one of the third

TABLE 3 Bond lengths obtained in the present simulations compared to previous molecular dynamics and experimental studies

Bond length (Å)			
	This study	**Previous MD work**	**Experiment**
Si-O	1.60	1.59[55]	1.52-1.85[56]; 1.60-1.65[57]
Ti-O	1.87-1.84	1.80[58]	1.85-1.95[56]; 1.69-1.97[57]
Ba-O	2.75-2.82	2.75-2.79[59]	2.75-2.89-[60]

TABLE 4 Oxygen coordination around glass formers for the different $BaO\text{-}TiO_2\text{-}SiO_2$ (BTS) glass compositions at 300 K

Coordination number							
	BTS-0	**BTS-5**	**BTS-10**	**BTS-15**	**BTS-20**	**BTS-25**	**BTS-30**
Si	4.01	4.00	4.00	4.00	4.00	4.00	4.01
Ti	—	5.15	5.02	5.10	5.10	4.98	5.03

peak of the RDF, which is considered as another added effect of TiO_2 on O-O bonds in the BTS glass. The Si-O, Ti-O, and Ba-O bond lengths were also calculated using the PDFs for each composition. When the TiO_2 content increases, the Si-O bond length did not change, the Ti-O bond showed a slight decrease while the Ba-O bond increased from 2.75 Å to 2.82 Å. Table 3 shows the main bonds length obtained in the BTS glass together with corresponding experimental values. The distances obtained by the present simulations show a good agreement with experimental observations and other molecular dynamics simulations (see Table 3).

Further information concerning the main structural units that built the BTS glass network can be derived by calculating the mean coordination number (CN) around the glass former elements (Silicon and Titanium). The PDFs of Si-O and Ti-O were integrated to the first minimum and the obtained values are reported for each composition in Table 4. This Table shows clearly that the basic structural units in the BTS glasses are mainly SiO_4 tetrahedra and TiO_5 pyramids. The addition of TiO_2 induces an important alteration of the CN of titanium compared to silicon, which suggests that the SiO_4 tetrahedra distribution is more stable than one of the TiO_5 pyramids.

To get additional information regarding the local structure in silicate glasses, we have used network statistics analysis. For instance, this technique allows to compute the fractions of different $Ti^{(n)}$ species (for n = 4, 5 and 6) present in the BTS glass network. Figure 3 shows the percentage number of $Ti^{(n)}$ species as a function of TiO_2 content. The sixfold and fourfold coordinated Ti species are found to be in low fractions while fivefold coordinated Ti takes the largest part of Ti species population. This behavior is consistent with previous experimental observations which suggest that Ti

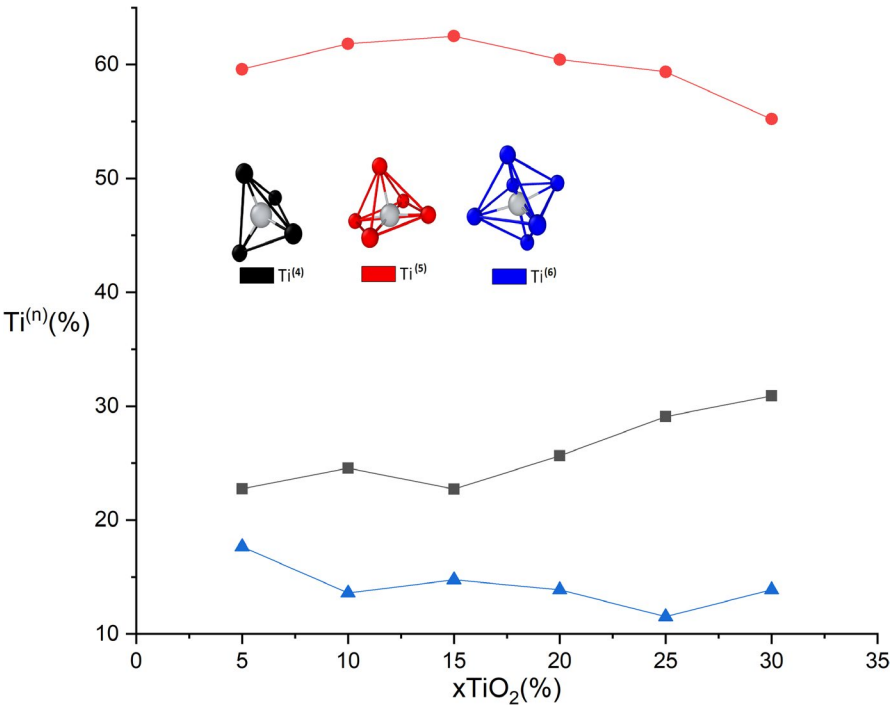

FIGURE 3 Ti species percentages as a function of the $BaO\text{-}TiO_2\text{-}SiO_2$ glass composition. On the right are shown examples of these Ti species [Color figure can be viewed at wileyonlinelibrary.com]

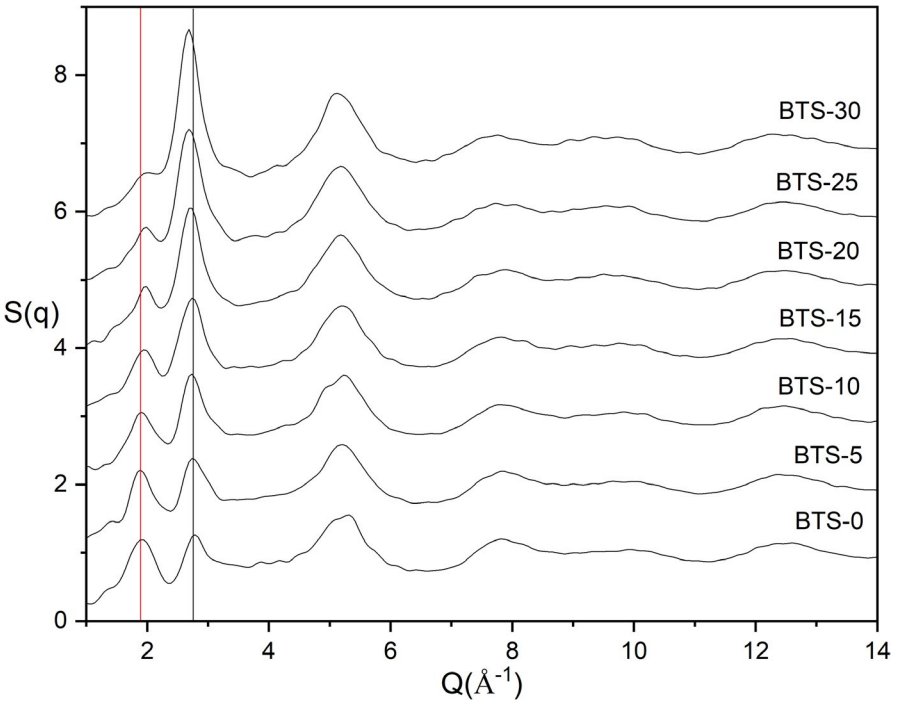

FIGURE 4 The total structure factors for the different simulated $BaO\text{-}TiO_2\text{-}SiO_2$ (BTS) glasses. Vertical lines are used to show the disappearance of the first peak (red) and to highlight the shift of the second peak as the TiO_2 content increases [Color figure can be viewed at wileyonlinelibrary.com]

is mainly fivefold coordinated[17] in BTS glasses. Increasing TiO_2 content in the system is accompanied by an increase in $Ti^{(4)}$ species and a decrease in $Ti^{(6)}$ species. However, for $Ti^{(5)}$ a maximum is reached at $x = 15\%$ followed by a decrease toward lower values. Compared to $x = 5\%$, the highest TiO_2 content (30%) has a lower population of $Ti^{(5)}$. Yet, this trend does not change the fact that the glass network remains homogeneous over a broad range of TiO_2 content.

3.2.2 | Medium range order

When studying structural properties of glasses, it is important to consider the different types of structural order that may be present in various length scales. In the previous section, the structural order present at distances <4 Å was found to be based on different types of polyhedra around network glass formers (Si, Ti) that define the basic units of the glass network. Pushing the structural order investigations at distances beyond 4 Å (intermediate range order) will provide a better understanding of the glass structural characteristics. A feature associated with the presence of intermediate range order is the presence of the first sharp diffraction peak (FSDP) in the total static structure factor. The origin of this peak is still a subject of debate to date. Indeed, many authors[40–42] have suggested several models to explain all observed anomalous characteristics such as the changes in the peak intensity and position with composition, temperature, and pressure.[43] In this study, the total static structure factor was calculated to understand the medium range order for all the compositions.

Figure 4 shows the total structure factor for all the simulated glasses, the main changes induced by composition are observed in the first three peaks. We see from this figure that as the content of TiO_2 increases from $x = 0\%$ to $x = 30\%$, the second peak intensity has significantly increased. This change is accompanied by the attenuation of the FSDP, which has changed from a significant peak in barium silicate glass to a second peak shoulder in high-TiO_2 content glasses. For the third peak, no significant change in the intensity was observed, but its shape has changed from an asymmetric peak to a more symmetric one. To understand the origin of those changes, we have calculated the partial structure factor (PSF) of the different pairs for the composition $x = 20\%$.

The decomposition of the structure factor depicted in Figure 5 shows that all atom pairs contribute to the FSDP, except for pairs with oxygen that give a small to a negligible contribution. Studies dedicated to explain the origin of the FSDP[42,44,45] have attributed its presence to the quasiperiodic fluctuation in atomic density that creates the ordering of interstitial voids in the structure. This explanation can help to understand the changes observed in the FSDP (Figure 4) as well as the observed increase in the glass density with the addition of TiO_2.

Figure 5 shows also that the PSF of Ba-Ba pair is the fastest decayed while the Si-Ti pair shows the slowest decay. This latter observation suggests a strong correlation between TiO_n polyhedra and SiO_4 tetrahedra. Otherwise, Figure 4 shows that almost all pairs contribute to the second peak intensity changes with an important contribution from O-O and Si-Ti pairs. Increasing TiO_2 content does not only change the peak intensity but shifts its position to lower q values as highlighted by the black line in Figure 4. This shift accompanied with a gain in intensity can be attributed to the increase in the amount of TiO_n polyhedra and the decrease in SiO_4 tetrahedra.

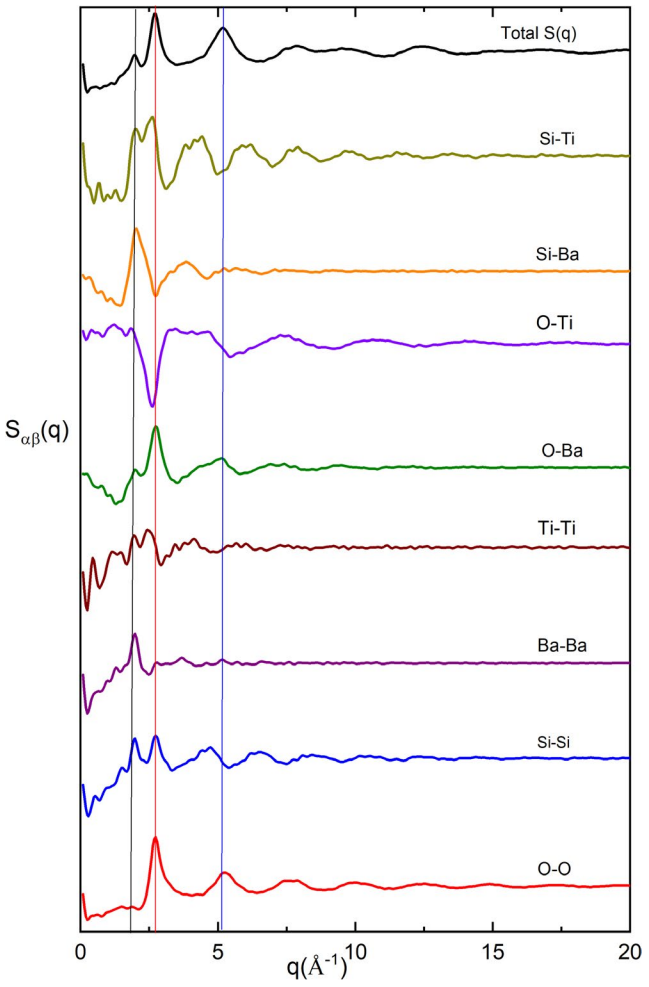

FIGURE 5 Partial structure factors of different pairs contributions for the $x = 20\%$ glass composition. Colored lines are eyes indication to the total structure factor peaks [Color figure can be viewed at wileyonlinelibrary.com]

3.2.3 | Network statistics

Glass network structures can hide many features under their amorphous state that can be revealed by studying their network statistics. In silicate glasses, coordination number around oxygens, rings statistics, and Q_n distribution can help to reveal what is special about a glass network and what gives it the founded properties. The coordination number around oxygens can explain how the connectivity changes with the composition and help to find the different type of linkages that maintain the glass network connectivity. Rings statistics define the size distribution of rings in glasses and characterize the nature of medium range structures. The distribution of Q_n species indicates the ordering of the glass network by finding how bridging oxygens (BOs) are distributed around the glass former elements.[46]

3.2.4 | Oxygens species and polyhedral linkage

Oxygen species are classified generally into four types: BOs which represent oxygens connected to two glass formers, nonbridging oxygens (NBOs) that stand for oxygens connected to one glass former, oxygen triclusters (TO) that connect three glass formers and finally free oxygens which represent oxygens connected to only glass modifiers. Table 5 shows the percentage of each oxygen type in the BTS glass. Three main observations can be made when adding TiO_2 to the glass. Firstly, free and tricluster oxygens are the rarest species in the network; they are present in amounts less than 1%. This behavior can be assigned to two effects: (a) the presence of some kind of structural defect due to the pair potential used in our simulations or to the high-cooling rate, (b) the neutralization of the extra charge around TiO_n polyhedra replacing the role of Ba^{2+}. When BaO concentration is higher than that of TiO_2, TO are not expected to exist in an observable quantity. The creation of this type of oxygen is considered as a mechanism of charge neutralization when the cation that should do it is lacking. In this investigation, the BaO content is large enough (30%) to compensate the charge around all Ti species, so we should expect a very small amount of TO. The second observation is related to bridging oxygens that represent the most dominant species in the glass. The increase in TiO_2 leads to the increase in connectivity in the network explained by the increase in bridging oxygens. The third observation is related to the population of NBOs that decrease without disappearing completely from the network. This trend can have many consequences on macroscopic properties of this glass such as the increase in glass transition temperature and viscosity.[47] Indeed, the experimental study of Mezeix et al[17] has shown these consequences as an effect of increasing TiO_2 content.

The impact of the BTS glass structure on macroscopic properties can also be attributed to the different types of bridging oxygens that define the interpolyhedron connectivity. Three types of bridging oxygens can be found: Ti-O-Ti, Ti-O-Si, and Si-O-Si, where the oxygen atom is bonded to two Ti atoms, one Ti atom and one Si atom, and to two Si atoms, respectively. Figure 6 shows how the amounts of these types of linkages evolve with the TiO_2 content. At low-TiO_2 content, Si-O-Si and Si-O-Ti are the most favored linkages while the Ti-O-Ti is not significant. When the TiO_2 content increases, we observe the Ti-O-Ti linkage more frequently. When TiO_2 content reaches $x = 20\%$, the Ti-O-Si linkage exceeds the Si-O-Si linkage in population and becomes the most contributing population of bridging oxygens. For TiO_2 contents beyond 20%, the amount of Si-O-Ti linkages shows a kind of saturation while the Si-O-Si linkage continues decreasing and being replaced by Ti-O-Ti. This can be attributed mainly to the abundance of Si atoms for low-TiO_2 contents favoring the Si-O bonds whereas for higher TiO_2 contents, Ti atoms replace Si thereby increasing the amount of Ti-O bonds.

Nonbridging oxygens can also be found in different types depending on which glass former the oxygen is connected to.

	BTS-0	BTS-5	BTS-10	BTS-15	BTS-20	BTS-25	BTS-30
FO (%)	0.01	0	0.02	0	0	0	0.06
BO (%)	64.20	67.55	70.06	72.80	74.76	76.37	78.95
NBO (%)	35.80	32.45	29.92	27.18	25.09	23.43	20.69
TO (%)	0	0	0.01	0.02	0.15	0.20	0.30

TABLE 5 Percentage of different oxygen species calculated for different $BaO-TiO_2-SiO_2$ (BTS) compositions from our glass samples obtained by MD simulations at 300 K

Two types of linkages are found in the BTS glass: Ba-O-Si (where O is connected to one Ba and one Si) and Ba-O-Ti (where O is connected to one Ba and one Ti). Table 6 shows the percentages of each type for different glass compositions. We observe from this Table that the percentage of Ba-O-Si has decreased from 97% (for 5% of TiO_2) to 72% (for 30% of TiO_2) while the percentage of Ba-O-Ti linkage has increased from 3% (for 5% of TiO_2) to 28% (for 30% of TiO_2). The increase in TiO_2 content as shown previously has lowered the number of NBOs, which is consistent with the decrease observed in Ba-O-Si linkages. Ba-O-Si and Ba-O-Ti linkages also show an important difference in populations even for high TiO_2 arisen from the fact that Ba-O-Si NBOs are more favorable in the BTS glass network independently from the composition changes. Table 6 also shows that Ba-O-Ti linkage percentage values are close to TiO_2 composition in the glass. This can strongly support the fact that TiO_n units are mainly present at the boundary between the network former and the network modifier regions, which is consistent with Farges[48] sketch regarding the structure of BTS glasses.

The cation modifier plays generally two roles in the glass network: (a) it can be a network modifier that depolymerizes the glass structure by segregating with NBOs and forming channels in the structure; or (b) a charge compensator that neutralizes the charge around the local environment of intermediate oxide units (like Ti here). The role of the cation modifier depends strongly on the composition and the ratio of the oxide modifier to the intermediate. For example in sodium aluminosilicate glasses, it has been observed[19,46] that when the ratio $[Al_2O_3]/[Na_2O]$ is close to 1 all sodium ions act as charge compensators of AlO_4 units and none of them will create NBOs, when the ratio is lower than 1 sodium ions act as both charge compensators of Al units and network modifiers. However, when the ratio is larger than 1 different mechanisms for sodium aluminosilicate are suggested to compensate the charge of Al units such as the formation of octahedral Al units[49] and oxygen triclusters.[50] In BTS glasses, the charge-balancing role of Ba^{2+} around Ti is not clear. Ti can be present in BTS glasses in the form of three coordination state, and it has been also demonstrated that the increase of TiO_2 content is not directly responsible for decreasing NBOs in the network as can be seen in Table 6. To get more insight into the NBOs distribution around Ti species and the role of Ba in the glass network, we have calculated the population of $Ba-O-Ti^{(n)}$ linkage in the BTS glass. Figure 7 shows the variation of these linkages as a function of TiO_2 content. At low

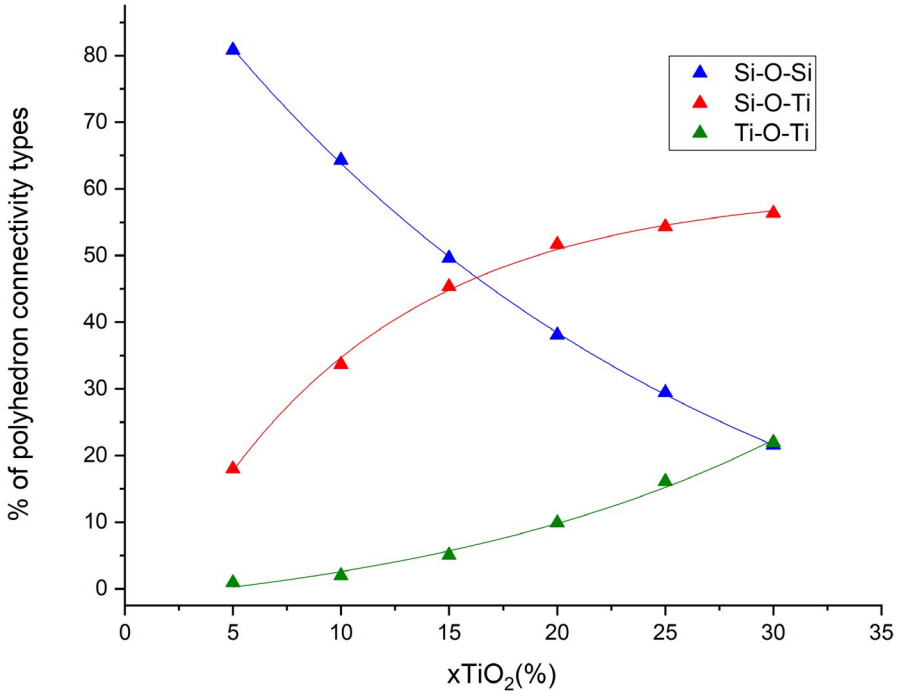

FIGURE 6 The percentage of the different bridging oxygen types as a function of the glass composition obtained from our MD simulations at 300 K [Color figure can be viewed at wileyonlinelibrary.com]

TABLE 6 Percentages of the different types of NBOs generated by our simulations at 300 K and averaged over 100 configuration

	BTS-5	BTS-10	BTS-15	BTS-20	BTS-25	BTS-30
Ba-O-Si	96.66	91.53	87.53	83.29	78.19	71.83
Ba-O-Ti	3.34	8.26	12.48	16.71	21.80	28.17

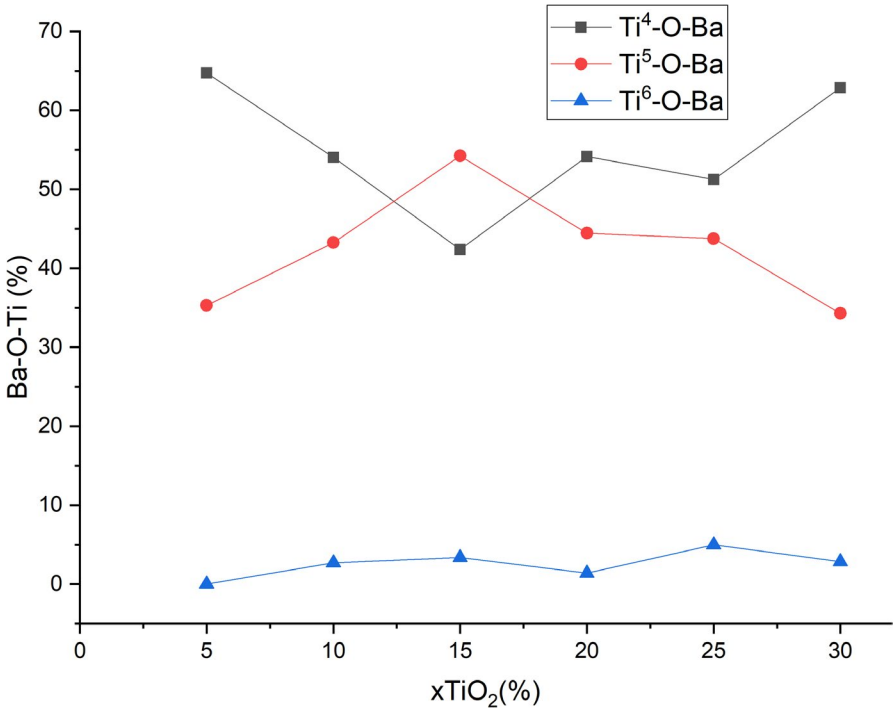

FIGURE 7 Ba-O-Ti linkage types evolution for different TiO_2 composition in $BaO\text{-}TiO_2\text{-}SiO_2$ glasses obtained at 300K and averaged over 100 configuration [Color figure can be viewed at wileyonlinelibrary.com]

TiO_2, TiO_4 is more surrounded by Ba^{2+} cations compared to TiO_5 and TiO_6. Upon increasing TiO_2, Ba^{2+} cations tend to get away from TiO_4 as observed by the decrease in Ba-O-$Ti^{(4)}$ population until reaching a minimum at $x = 15\%$ and then switch its trend to increasing, while Ba-O-$Ti^{(5)}$ linkages show the opposite trend. For Ba-O-$Ti^{(6)}$, no effective change was observed since its population is negligible. To further discuss these results, it is worth noting that TiO_4 tetrahedra are charge neutral while TiO_5 pyramid squares are not. Hence, the charge-balancing role of Ba^{2+} cations around each TiO_n species depends on whether its charge is neutral or not. When Ti is in its tetrahedral form, the four surrounding oxygens neutralize Ti^{4+} charge, which makes Ba^{2+} cations playing the role of network modifiers. For the pyramidal form of Ti, there exists an excess of charge that should be compensated by another cation, which identifies Ba^{2+} as charge-balancing cations. When Ti is in an octahedral form, the charge excess is −2 but as showed in Figure 7 it is extremely rare to find any Ba^{2+} cation around it, and if ever found, Ba^{2+} will act as a charge-balancing cation. Thus, the presence of TiO_6 in the BTS glass can be considered as a consequence of nonneutralized charge of TiO_5 that should be present in the border of the network forming region following the sketching of Farges et al[48] and it has been found to be inside it. Keeping BaO content fixed has also some consequences on the main role of Ba^{2+} in BTS glasses. The decrease observed in Ba-O-$Ti^{(5)}$ linkages that represent the charge-balancing role of Ba^{2+} cations is directly related to the decrease in NBOs and to the fact that TiO_5 is more involved in building up the glass network backbone. This can be confirmed by the increase in Q_5 proportion (See Figure 9). These changes make the charge-balancing role less necessary and thus the remaining Ba^{2+} cations will continue to be network modifiers and increase their number compared to the charge balancing one as shown in Figure 7.

3.2.5 | Q_n species distribution

The Q_n species distribution can give some information on the linkage of the basic building units of the glass network. A Q_n species represents the environment of the glass former (Si or Ti in the present study) in terms of n bridging oxygen. Figure 8 represents an example of Q_6 species found in the BTS glass. It will help to describe the change brought by TiO_2 in the glass network at intermediate range order. In our MD simulations, Q_3 and Q_4 species represent the main groups that contribute in building up the network of the BTS glass at low TiO_2 (Figure 9A) with the amount of Q_3 species larger than

that of Q_4 species. When the TiO_2 content increases up to $x = 15\%$, Q_4 species grow up at the expense of Q_3 species. The presence of Q_2 maintains the equilibrium of this species following the well-known disproportion equation defined as:

$$2Q_n \Leftrightarrow Q_{n-1} + Q_{n+1}$$

These Q_n distributions have also been characterized by Raman spectroscopy.[17] Not only the Q_3 predominance at low TiO_2 has been observed but also the conversion from Q_3 to Q_2 and Q_4 with increasing TiO_2 has been shown. The presence of other Q_n species such as Q_5 and Q_6 is also a consequence of adding TiO_2 to the glass network. Due to the existence of fivefold and sixfold coordinated titanium, the TiO_5 and TiO_6 expose themselves as Q_5 and Q_6. Hence, the dependence of Q_5 and Q_6 on glass composition is the same as that of TiO_5 and TiO_6 polyhedra. As can be seen in Figure 9A, two classes of species can be identified showing opposite trends, those with a low number of bridging oxygens ($n < 4$) and the others with a high number of bridging oxygens ($n \geq 4$). The Q_1, Q_2 and Q_3 populations continue to decrease with a dependence on SiO_2 while the others (Q_4, Q_5 and Q_6) rapidly increase with TiO_2. There is also the fact that SiO_4 tetrahedra attract more Ba^{2+} cations than TiO_n polyhedra and thus fewer bridging oxygens will surround Si compared to Ti.

A further analysis was also conducted in the aim to elucidate the contribution of each glass former by calculating the partial population of Q_n for Si and Ti. The results are depicted in Figure 9B,C. There exists a disproportion between the two most abundant Q_n species for both Si and Ti. For Si-based Q_n species, the population of Q_3 and Q_4 is stable upon increasing TiO_2 until reaching 25% where they intersect. For Ti-based Q_n species, the population of Q_4 and Q_5 do not show a clear evolution and compared to that relative Si.

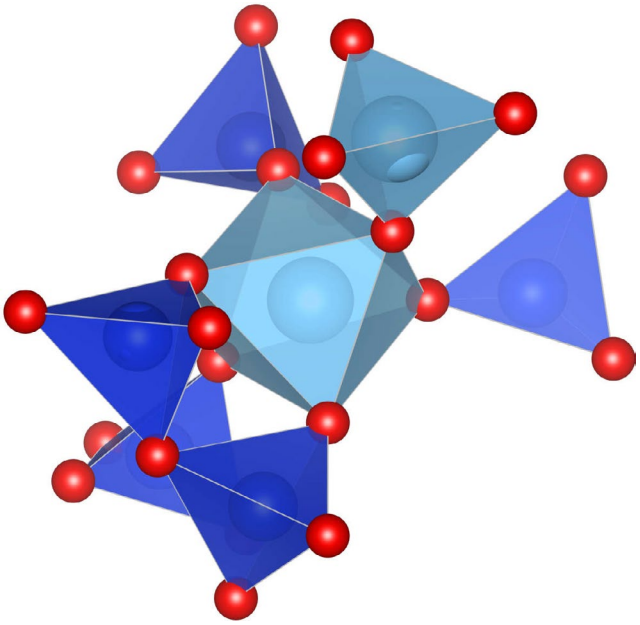

FIGURE 8 Snapshot of Q_6, pictured using VESTA,[51] observed in the $BaO\text{-}TiO_2\text{-}SiO_2$ glass with a TiO_6 octahedron surrounded by one TiO_4 and five SiO_4 tetrahedra. The red balls represent oxygen, silicon atoms are found in the center of the purple colored tetrahedra and titanium atoms are in the center of the blue colored remaining polyhedra [Color figure can be viewed at wileyonlinelibrary.com]

3.2.6 | Ring statistics

The ring size distribution calculated for the BTS glasses is represented in Figure 10. The presence of the medium range order confirmed by the FSDP is highlighted using rings statistics. The rings are defined as closed paths made by T

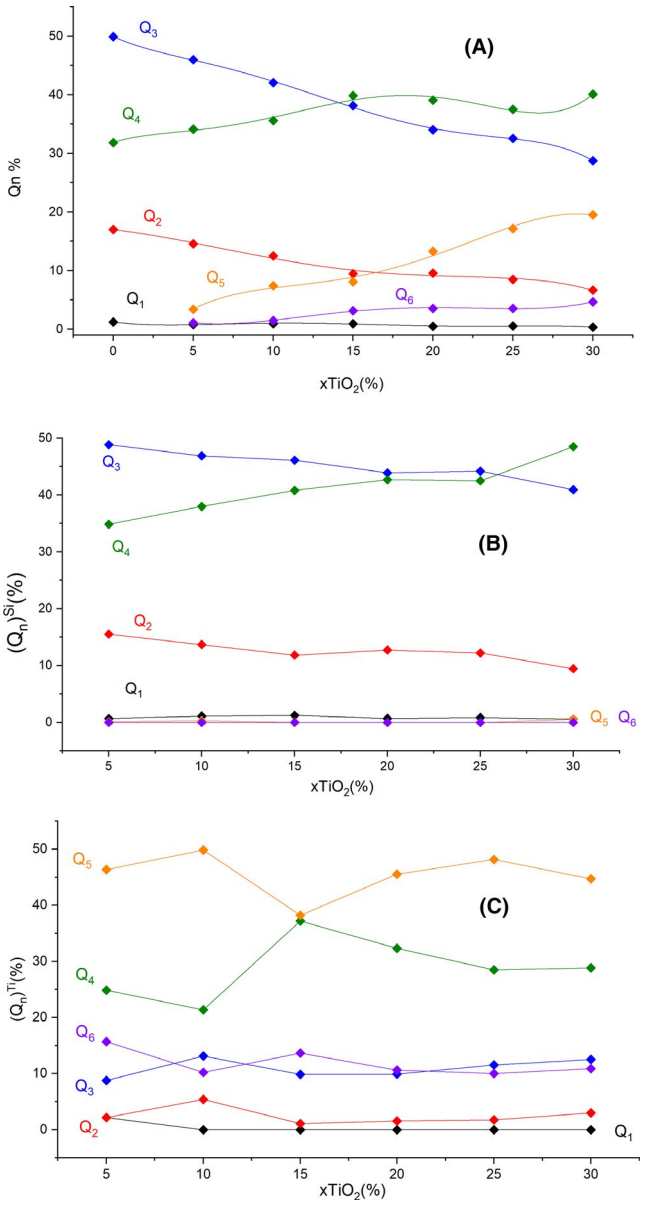

FIGURE 9 (A), Q_n percentages for the different glass compositions obtained from our simulations at 300 K. Fitted lines serve as guide for the eyes. (B), Si and (C) Ti based Q_n species population [Color figure can be viewed at wileyonlinelibrary.com]

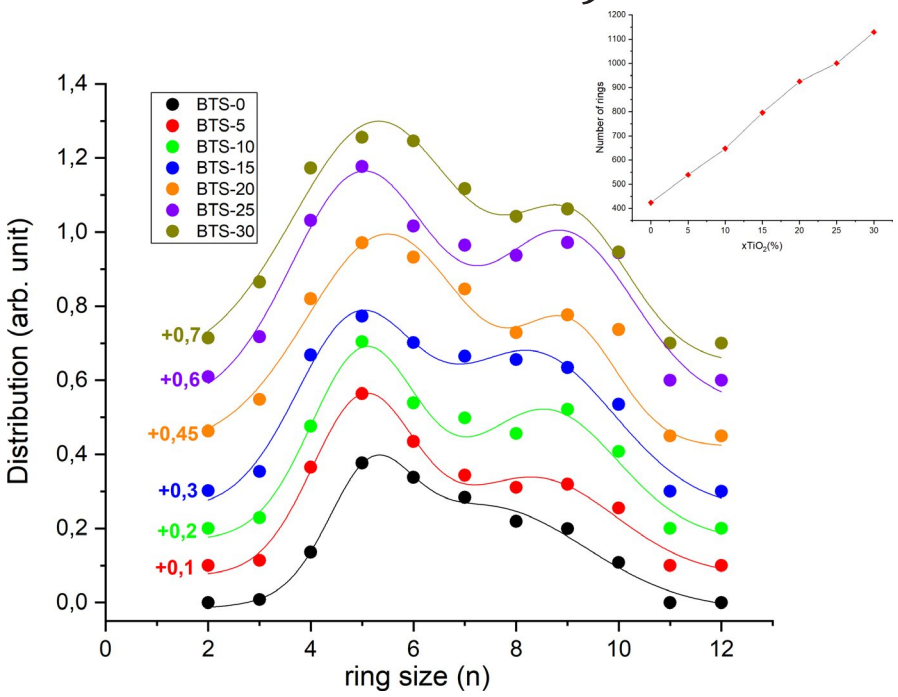

FIGURE 10 Ring size distribution for the different BaO-TiO_2-SiO_2 (BTS) glass compositions from MD simulations at 300 K. Fitted lines are guide for the eyes. The inset shows the evolution of rings number [Color figure can be viewed at wileyonlinelibrary.com]

(T = Si,Ti) nodes and linked by oxygen atoms. The rings size distribution (Figure 10) shows a bimodal distribution around 5- and 9-membered rings. It can be seen that increasing TiO_2 content intensifies both peaks (with a higher rate for the first peak) which means that the number of rings increases with TiO_2. This observation can be related to the glass connectivity that has increased by the increase in BOs, those latter enhance the creation of closed paths. The bimodal distribution of rings observed here is a general feature observed in many alkali and alkaline-earth silicate,[31,51] the main characteristic of the two peaks is seen in Ti-free glass which means that TiO_2 does not have any contribution to their shape. In crystalline fresnoite, the TiO_5 pyramid and the Si_2O_7 groups are linked into "heterocyclic" 5-membered rings,[52] the increase in this type of rings in BTS glasses with TiO_2 content may lead to conclude that the role of this oxide is to increase order. The population of 5- and 9-membered rings that has changed with TiO_2 can also suggest that two regions are present in the glass: (a) a first one related to the glass polymerized region and (b) a second one that represents the Ba-rich region surrounded by a 9-membered ring.

The ring size distribution can also reveal the difference in the glass-forming ability.[53] In BTS glasses, it has been found[17] that BTS-0 composition has the lowest fragility and thus the highest glass forming ability following Angell's classification.[54] The presence of large rings at low-TiO_2 content can be understood in terms of topological order-disorder. According to Kohara et al,[51] silica-rich composition with high glass forming ability exhibits a higher topological disorder compared to silica poor glass. This is due to the observed broadness of the ring size distribution that increases the glass structural heterogeneity leading to high topological disorder compared to glasses with lower glass forming ability. This can confirm that increasing TiO_2 composition increases structural order of BTS glasses.

4 | CONCLUSION

The structural and elastic properties of a series of barium titanosilicate glasses were investigated using molecular dynamics simulations. The results show that TiO_2 increases the glass elasticity with a very good agreement between MD and experimental data. This increase was accompanied by structure-induced changes caused by the different Ti coordination states with the predomination of fivefold coordinated Ti. The increase in TiO_2 content has made the glass network more connected as shown by the changes in oxygens environment. The characterized structural models have a clear increase in bridging oxygens with favored Si-O-Ti linkages at high-TiO_2 contents and Si-O-Si linkages at low-TiO_2 contents. The medium range order was also studied using structure factor and rings statistics. The results showed an increase in rings number presenting coherent conclusions about the observed increase in connectivity with increasing the TiO_2 content. The Q_n distribution was presented to define the polyhedra aggregation in the network; this distribution has showed a qualitative agreement with experimental observations. The studied structural models have showed a good agreement with Farges[48] structural models built on high resolution XANES spectroscopy experiment. In the barium titanosilicate glass, the main changes in the glass structure are found to be in the intermediate range order. Those changes were found to increase the topological order but decrease the glass

forming ability. Finding a way to increase it will facilitate the BTS glass-ceramics material production in industry and thus replace many materials that have regrettable environmental impacts. Our study can be considered as a step toward a clear view of the effect of TiO_2 on the BTS glass intermediate range order.

ORCID

El Mehdi Ghardi https://orcid.org/0000-0003-0658-7431

REFERENCES

1. Calvez L. 10-Transparent chalcogenide glass-ceramics. In: Adam J-L, Zhang XBT-CG, editors. Chalcogenide glasses: Preparation, properties and applications. Oxford: Woodhead Publishing, 2014; p. 310–43. http://www.sciencedirect.com/science/article/pii/B9780857093455500106
2. Upadhyaya GS, Holland W, Beall G. Glass-ceramic technology, "The American Ceramic Society". Westerville, OH: International Institute for the Science of Sintering, 2002; p. 372. Vol. 36, Science of Sintering. 2004.
3. Wisniewski W, Döhler F, Rüssel C. Oriented nucleation and crystal growth of Ba-fresnoite ($Ba_2TiSi_2O_8$) in 2 BaO TiO_2 $2SiO_2$ Glasses with Additional SiO_2. Cryst Growth Des. 2018;18(5):3202–8. http://pubs.acs.org/doi/10.1021/acs.cgd.8b00312.
4. Masai H, Okada G, Kawaguchi N, Yanagida T. Photoluminescence and X-ray-induced scintillation of BaO-TiO2-SiO2 glasses and the glass-ceramics. J Non Cryst Solids. 2018;501:131–5.
5. Park TJ, Davis MJ, Vullo P, Nenoff TM, Krumhansl JL, Navrotsky A. Thermochemistry and aqueous durability of ternary glass forming Ba-titanosilicates: fresnoite ($Ba_2TiSi_2O_8$) and Ba-titanite ($BaTiSiO_5$). J Am Ceram Soc. 2009;92(9):2053–8.
6. Abdel-Baki M, El-Diasty F. Optical properties of oxide glasses containing transition metals: case of titanium- and chromium-containing glasses. Curr Opin Solid State Mater Sci. 2006;10(5-6):217–29. https://doi.org/10.1016/j.cossms.2007.08.001
7. Roberts MA, Sankar G, Thomas JM, Jones RH, Du H, Chen J, et al. Synthesis and structure of a layered titanosilicate catalyst with five-coordinate titanium. Nature. 1996;381(6581):401–4. https://doi.org/10.1038/381401a0
8. Xu H, Navrotsky A, Nenoff M, Nyman TM. Thermochemistry of framework titanosilicate $A_2TiSi_6O_{15}$ (A=K, Rb, Cs). J Am Ceram Soc. 2005;88(7):1819–25. https://doi.org/10.1111/j.1551-2916.2005.00275.x
9. Viani A, Palermo A, Zanardi S, Demitri N, Petrícek V, Varini F, et al. Structure and stability of BaTiSi2O7. Acta Crystallogr Sect B Struct Sci Cryst Eng Mater. 2015;71:153–63.
10. Taylor NT, Davies FH, Hepplestone SP. First principles electronic and elastic properties of fresnoite Ba2TiSi2O8. Mater Res Express. 2017;4(12):125904.
11. Wisniewski W, Nagel M, Völksch G, Rüssel C. Electron backscatter diffraction of fresnoite crystals grown from the surface of a $2BaO{\cdot}TiO_2{\cdot}2.75SiO_2$ Glass. Cryst Growth Des. 2010;10(3):1414–8. https://doi.org/10.1021/cg901407d.
12. Nakamura K, Takahashi Y, Fujiwara T. Lowerature excess heat capacity in fresnoite glass and crystal. Sci Rep. 2014;4:8–11.
13. Masai H, Tsuji S, Fujiwara T, Benino Y, Komatsu T. Structure and non-linear optical properties of BaO-TiO_2-SiO_2 glass containing $Ba_2TiSi_2O_8$ crystal. J Non Cryst Solids. 2007;353(22–23):2258–62.
14. Cabral AA, Fokin VM, Zanotto ED, Chinaglia CR. Nanocrystallization of fresnoite glass. I. nucleation and growth kinetics. J Non Cryst Solids. 2003;330(1):174–86. http://www.sciencedirect.com/science/article/pii/S0022309303006124
15. Bang NJ, Cho JH, Vano YS. The Crystallization mechanism and dielectric property of BaTiO~ 3-SiO~ 2 glass. J Korean Phys Soc. 1998;32:S845–S849.
16. Masai H, Tsuji S, Fujiwara T, Benino Y, Komatsu T. Structure and non-linear optical properties of BaO–TiO_2–SiO_2 glass containing $Ba_2TiSi_2O_8$ crystal. J Non Cryst Solids. 2007;353(22–23):2258–62.
17. Mezeix P, Célarié F, Houizot P, Gueguen Y, Muñoz F, Rouxel T. Elasticity and viscosity of BaO-TiO_2-SiO_2 glasses in the 0.9 to 1.2Tg temperature interval. J Non Cryst Solids. 2016;446:45–52. https://doi.org/10.1016/j.jnoncrysol.2016.05.006
18. Kim JE, Kim SJ, Yang YS. Dielectric and conduction behavior of $xBaTiO_3{\cdot}(1\text{-}x)$ SiO_2 glasses. Mater Sci Eng A. 2001;304:487–90.
19. Mysem B, Richet P. (editors). Subject index. Silicate glasses and Melts [Internet]. Elsevier, 2005; p. 525–44. http://www.sciencedirect.com/science/article/pii/S0921319805800389
20. Jabraoui H, Vaills Y, Hasnaoui A, Badawi M, Ouaskit S. Effect of sodium oxide modifier on structural and elastic properties of silicate glass. J Phys Chem B. 2016;120(51):13193–205.
21. Jabraoui H, Malki M, Hasnaoui A, Badawi M, Ouaskit S, Lebègue S, et al. Thermodynamic and structural properties of binary calcium silicate glasses: insights from molecular dynamics. Phys Chem Chem Phys. 2017;19(29):19083–93. http://xlink.rsc.org/?DOI=C7CP03397D
22. Trady S, Hasnaoui A, Mazroui M, Saadouni K. Local atomic structures of single-component metallic glasses. Eur Phys J B. 2016;89(10):223.
23. Kbirou M, Trady S, Hasnaoui A, Mazroui M. Cooling rate dependence and local structure in aluminum monatomic metallic glass. Philos Mag. 2017;97(30):2753–71. https://doi.org/10.1080/14786435.2017.1352107
24. Kbirou M, Mazroui M, Hasnaoui A. Atomic packing and fractal behavior of Al-Co metallic glasses. J Alloys Compd. 2018;735:464–72.
25. Pedone A, Malavasi G, Menziani MC, Cormack AN, Segre U. A new selft-consistent empirical interatomic potential model for oxides, silicates and silica-based glasses. J Phys Chem B. 2006;110:11780–95.
26. Habasaki J, Casalini R, Ngai KL. Molecular dynamics study of thermodynamic scaling of the glass-transition dynamics in ionic liquids over wide temperature and pressure ranges. J Phys Chem B. 2010;114(11):3902–11.
27. Habasaki J, Leon C,Ngai KL. Dynamics of glassy, crystalline and liquid ionic conductors. Top Appl Phys. 2017;132:355–410.
28. Hansen J-P, McDonald IDR. Theory of simple liquids, 4th ed. New York: Academic Press, 2013; p. 636.
29. Faber TE, Ziman JM. A theory of the electrical properties of liquid metals. Philos Mag. 1964;11:153–73. http://adsabs.harvard.edu/cgi-bin/nph-data_query?bibcode=1965PMag.11.153F&link_type=EJOURNAL
30. King SV. Ring configurations in a random network model of vitreous silica. Nature. 1967;213(5081):1112.

31. Yuan X, Cormack AN. Efficient algorithm for primitive ring statistics in topological networks. Comput Mater Sci. 2002;24(3):343–60.
32. Goetzke K, Klein H-J. Properties and efficient algorithmic determination of different classes of rings in finite and infinite polyhedral networks. J Non Cryst Solids. 1991;127(2):215–20.
33. Le Roux S, Jund P. Ring statistics analysis of topological networks: new approach and application to amorphous GeS_2 and SiO_2 systems. Comput Mater Sci. 2010;49(1):70–83.
34. Timoshenko S, Goodier JN. Theory of Elasticity [Internet]. Hill M, editor. Vol. 49, Journal of Elasticity. 1986; p. 143–427. http://www.amazon.com/Elasticity-McGraw-Hill-Classic-Textbook-Reissue/dp/0070858055
35. Deschamps T, Margueritat J, Martinet C, Mermet A, Champagnon B. Elastic moduli of permanently densified silica glasses. Sci Rep. 2014;4:1–7.
36. Vogel W. Glass chemistry [Internet]. 2nd ed. Vogel W, editor. Berlin, Heidelberg: Springer, 1994; p. 464. http://link.springer.com/10.1007/978-3-642-78723-2
37. Scannell G, Koike A, Huang L. Structure and thermo-mechanical response of TiO_2-SiO_2 glasses to temperature. J Non-Cryst Solids. 2016;447:238–47.
38. Sandstrom DR, Lytle FW, Wei PSP, Greegor RB, Wong J, Schultz P. Coordination of Ti in TiO_2-SiO_2 glass by X-ray absorption spectroscopy. J Non Cryst Solids. 1980;41(2):201–7. http://linkinghub.elsevier.com/retrieve/pii/0022309380901659
39. Scannell G, Huang L. Structure and thermo-mechanical response of Na_2O-TiO_2-SiO_2 glasses to temperature. J Non Cryst Solids. 2016;453:238–47.
40. Christie JK, Taraskin SN, Elliott SR. Structural characteristics of positionally disordered lattices: relation to the first sharp diffraction peak in glasses. Phys Rev B Condens Matter Mater Phys. 2004;70(13):1–5.
41. Salmon PS, Martin RA, Mason PE, Cuello GJ. Topological versus chemical ordering in network glasses at intermediate and extended length scales. Nature. 2005;435(7038):75–8.
42. Elliott SR. Origin of the first sharp diffraction peak in the structure factor of covalent glasses. Phys Rev Lett. 1991;67(6):711–4.
43. Crupi C, Carini G, González M, D'Angelo G. Origin of the first sharp diffraction peak in glasses. Phys Rev B. 2015;92(13):134206. https://doi.org/10.1103/PhysRevB.92.134206
44. Blétry J. Sphere and distance models for binary disordered systems. Philos Mag B. 1990;62(5):469–508. https://www.tandfonline.com/doi/full/10.1080/13642819008215248
45. Elliott SR. Interpretation of the principal diffraction peak of liquid and amorphous water. J Chem Phys. 1995;103(7):2758–61.
46. Xiang Y, Du J, Smedskjaer MM, Mauro JC. Structure and properties of sodium aluminosilicate glasses from molecular dynamics simulations. J Chem Phys. 2013;139(4):044507. https://doi.org/10.1063/1.4816378
47. Lusvardi G, Malavasi G, Tarsitano F, Menabue L, Menziani MC, Pedone A. Quantitative structure-property relationships of potentially bioactive fluoro phospho-silicate glasses. J Phys Chem B. 2009;113(30):10331–8.
48. Farges F. Coordination of Ti in crystalline and glassy fresnoites: a high-resolution XANES spectroscopy study at the Ti K-edge. J Non Cryst Solids. 1996;204(1):53–64. http://www.sciencedirect.com/science/article/pii/0022309396003924
49. Moore H, McMillan PW. A study of glasses consisting of the oxides of elements of low atomic weight. J Soc Glas Tech. 1956;40:66T–161T.
50. Lacy ED. Aluminum in glasses and melts. Phys Chem Glas. 1963;4(6):234–8.
51. Kohara S, Akola J, Morita H, Suzuya K, Weber JKR, Wilding MC, et al. Relationship between topological order and glass forming ability in densely packed enstatite and forsterite composition glasses. Proc Nat Acad Sci. 2011;108(36):14780–5. https://doi.org/10.1073/pnas.1104692108
52. Waltersson K. The crystal structure of $Cs_2V_5O_{13}$. Acta Crystallog Sec B. 1977;33(3):784–9. https://doi.org/10.1107/S0567740877004646
53. Akola J, Kohara S, Ohara K, Fujiwara A, Watanabe Y, Masuno A, et al. Network topology for the formation of solvated electrons in binary CaO-Al2O3 composition glasses. Proc Natl Acad Sci. 2013;110(25):10129–34. http://www.pnas.org/cgi/doi/10.1073/pnas.1300908110
54. Angell CA. Formation of glasses from liquids and biopolymers. Science. 1995;267(1924):1924–35. https://doi.org/10.1126/science.267.5206.1924
55. Rai M, Mountjoy G. Molecular dynamics modelling of the structure of barium silicate glasses BaO–SiO_2. J Non Cryst Solids. 2014;401:159–63. https://doi.org/10.1016/j.jnoncrysol.2013.12.026
56. Ochi Y. Fresnoite crystal structure in glass-ceramics. Mater Res Bull. 2006;41(4):740–50.
57. Markgraf SA, Halliyal A, Bhalla AS, Newnham RE, Prewitt CT. X-ray structure refinement and pyroelectric investigation of fresnoite, $Ba_2TiSi_2O_8$. Ferroelectrics. 1985;62(1):17–26.
58. Bernard C, Chaussedent S, Monteil A, Ferrari M. Molecular dynamics simulation of an erbium-activated titania-silica glass: composition influence on the structural properties. Philos Mag B Phys Condens Matter; Stat Mech Electron Opt Magn Prop. 2002;82(6):681–93.
59. Sio B, Rai M, Mountjoy G. Molecular dynamics modelling of the structure of barium silicate. J Non Cryst Solids. 2014;401:10–4.
60. Muller E, Heide K, Zanotto ED. Molecular structure and nucleation in silicate glasses. J Non Cryst Solids. 1993;155(1):56–66.

How to cite this article: Ghardi EM, Atila A, Badawi M, Hasnaoui A, Ouaskit S. Computational insights into the structure of barium titanosilicate glasses. *J Am Ceram Soc*. 2019;102:6626–6639. https://doi.org/10.1111/jace.16536